

**SPACE MAPPING OPTIMIZATION
OF WAVEGUIDE FILTERS
USING FINITE ELEMENT
AND MODE-MATCHING
ELECTROMAGNETIC SIMULATORS**

J.W. Bandler, R.M. Biernacki,
S.H. Chen and D. Omeragić

SOS-97-6-R

March 21, 1997

© J.W. Bandler, R.M. Biernacki, S.H. Chen and D. Omeragic 1997

No part of this document may be copied, translated, transcribed or entered in any form into any machine without written permission. Address enquiries in this regard to Dr. J.W. Bandler. Excerpts may be quoted for scholarly purposes with full acknowledgement of source. This document may not be lent or circulated without this title page and its original cover.

SPACE MAPPING OPTIMIZATION OF WAVEGUIDE FILTERS USING FINITE ELEMENT AND MODE-MATCHING ELECTROMAGNETIC SIMULATORS

John W. Bandler, *Fellow, IEEE*, Radoslaw M. Biernacki, *Fellow, IEEE*,
Shao Hua Chen, *Senior Member, IEEE*, and Dževat Omeragić, *Member, IEEE*

Abstract

For the first time in design optimization of microwave circuits, the aggressive space mapping (SM) optimization technique is applied to automatically align electromagnetic (EM) models based on hybrid mode-matching/network theory simulations with models based on finite-element (FEM) simulations. SM optimization of an H-plane resonator filter with rounded corners illustrates the advantages as well as the challenges of the approach. The parameter extraction phase of SM is given special attention. The impact of selecting responses and error functions on the convergence and uniqueness of parameter extraction is discussed. A statistical approach to parameter extraction involving ℓ_1 and penalty concepts facilitates a key requirement by SM for uniqueness and consistency. A multi-point parameter extraction approach to sharpening the solution uniqueness and improving the SM convergence is also introduced. Once the mapping is established, the effects of manufacturing tolerances are rapidly estimated with the FEM accuracy. SM has also been successfully applied to optimize waveguide transformers using two hybrid mode-matching/network theory models: a coarse one using very few modes and a fine model using many modes to represent discontinuities.

This work was supported in part by Optimization Systems Associates Inc. and in part by the Natural Sciences and Engineering Research Council of Canada under Grants OGP0007239, OGP0042444 and STR0167080, through the Micronet Network of Centres of Excellence, and through an Industrial Research Fellowship granted to Dr. Omeragić.

J.W. Bandler, R.M. Biernacki and S.H. Chen are with the Simulation Optimization Systems Research Laboratory and the Department of Electrical and Computer Engineering, McMaster University, Hamilton, Canada L8S 4L7. They are also with Optimization Systems Associates Inc., P.O. Box 8083, Dundas, Ontario, Canada L9H 5E7.

D. Omeragić is with Optimization Systems Associates Inc., P.O. Box 8083, Dundas, Ontario, Canada L9H 5E7.

I. INTRODUCTION

Direct exploitation of electromagnetic (EM) simulators in the optimization of arbitrarily shaped 3D structures at high frequencies is crucial for first-pass success CAD [1,2]. Recently, we reported successful automated design optimization of 3D structures using FEM simulations [1,3].

The objective of space mapping [3-5] is to avoid direct optimization of computationally intensive models. In this paper, for the first time, the aggressive space mapping optimization is applied to automatically align the results of two separate EM simulation systems. The RWGMM library [6,7] of waveguide models based on the mode matching (MM) technique [6-8] is used for fast/coarse simulations in the so-called optimization space \mathbf{X}_{os} . The library is linked to the network theory optimizers of OSA90/hope [9]. Maxwell Eminence [10] simulations accessed through Empipe3D [9] serve as the "fine" model in the so-called \mathbf{X}_{em} space. The space mapping procedure executes all these systems concurrently.

Both RWGMM and Maxwell Eminence provide accurate EM analysis. RWGMM is computationally efficient in its treatment of a variety of predefined geometries. It is ideally suited for modeling complex waveguide structures that can be decomposed into the available library building blocks. FEM-based simulators [11,12] such as Maxwell Eminence [10,12] are able to analyze arbitrary shapes, but they are computationally very intensive.

Aggressive space mapping optimization of an H-plane resonator filter with rounded corners is carried out. These rounded corners make RWGMM simulations somewhat less accurate. Once the mapping is established, subsequent Monte Carlo analysis of manufacturing tolerances exploits the FEM-based space mapped model with the speed of the MM/network theory simulator. To illustrate the flexibility in selecting the \mathbf{X}_{em} and \mathbf{X}_{os} models, space mapping is also applied to optimize waveguide transformers using two hybrid MM/network theory models: a coarse one using very few modes and a fine model using many modes to represent the discontinuities.

The parameter extraction phase is the key to effective space mapping optimization. The methodology, however, is sensitive to nonunique solutions or local minima inconsistent with the aimed solution. An in-depth study of this phenomenon is presented and ways to overcome such problems are addressed. We show that, at the expense of increased simulations of the fast coarse model, we can satisfy the requirement for uniqueness and consistency. We investigate how the choice of error functions influences the convergence and uniqueness of parameter extraction. We offer a solution based on statistical parameter extraction involving a powerful l_1 algorithm and penalty function concepts. We

introduce a multi-point parameter extraction approach to sharpening the solution uniqueness and improving the space mapping convergence in the automated design of a waveguide transformer.

II. FULLY AUTOMATED SPACE MAPPING OPTIMIZATION

By inspecting the steps involved in space mapping optimization [3,4], we recognize that the parameter extraction process is explicitly dependent on the specific models involved. In the flow diagram shown in Fig. 1 the MM waveguide library serves as the \mathbf{X}_{os} model and the FEM simulator as the \mathbf{X}_{em} model. The other steps of space mapping can be implemented within a generic layer of iterations. Following this guideline, the aggressive space mapping strategy has been fully automated using a two-level Datapipe architecture [9,13]. Fig. 1 illustrates the two iterative loops involving two different sets of variables. The outer loop updates the optimization variables \mathbf{x}_{em} of the \mathbf{X}_{em} model based on the latest mapping. The inner, dotted block, extracts the parameters \mathbf{x}_{os} of the \mathbf{X}_{os} model while \mathbf{x}_{em}^i is held constant. The Datapipe techniques allow us to carry out the nested optimization loops in two separate processes while maintaining a functional link between their results (e.g., the next increment to \mathbf{x}_{em} is a function of the results of parameter extraction).

Within the inner loop of parameter extraction, we can also utilize the Datapipe technique to connect external model simulators to the optimization environment (e.g., the Empipe3D system is a specialized Datapipe interface to Maxwell Eminence). Further details of the parameter extraction step will be elaborated in Sections IV through VII.

III. SPACE MAPPING OPTIMIZATION USING MM/NETWORK THEORY AND FEM

We address the design of the H-plane resonator filter with rounded corners shown in Fig. 2(b). The waveguide cross-section is 15.8×7.9 mm, while the thickness of the irises is $t = 0.4$ mm. The radius of the corners is $R = 1$ mm. The iris and resonator dimensions d_1, d_2, l_1, l_2 are selected as the optimization variables.

First, minimax optimization of the X_{os} model (Fig. 2(a)) is performed exploring the waveguide MM library with the following specifications provided by Arndt [14]

$$|S_{21}| < -35 \text{ dB} \quad \text{for} \quad 13.5 \text{ GHz} \leq f \leq 13.6 \text{ GHz}$$

$$|S_{11}| < -20 \text{ dB} \quad \text{for} \quad 14.0 \text{ GHz} \leq f \leq 14.2 \text{ GHz}$$

$$|S_{21}| < -35 \text{ dB} \quad \text{for} \quad 14.6 \text{ GHz} \leq f \leq 14.8 \text{ GHz}$$

where f represents the frequency.

The minimax solution \mathbf{x}_{os}^* is $d_1 = 6.04541$, $d_2 = 3.21811$, $l_1 = 13.0688$ and $l_2 = 13.8841$. It yields the target response for space mapping. At this point, the fine model X_{em} is analyzed by FEM using the \mathbf{x}_{os}^* values. The corresponding responses of the FEM model and hybrid mode-matching/network theory models are shown in Fig. 3. Focusing on the passband, we treat responses in the region $13.96 \leq f \leq 14.24$ GHz. The passband responses of both models at the point \mathbf{x}_{os}^* are shown in Fig. 4. Some discrepancy is evident.

Tables I and II summarize the steps of the successful space mapping optimization. The solution, corresponding to point $d_1 = 6.17557$, $d_2 = 3.29058$, $l_1 = 13.0282$ and $l_2 = 13.8841$, shown in Fig. 5 was obtained after only four Maxwell Eminence simulations, each with only fifteen frequency points. The space mapping results were verified by directly optimizing the H-plane filter using Empipe3D driving the Maxwell Eminence solver. Essentially the same solution was found.

IV. ERROR FUNCTIONS FOR PARAMETER EXTRACTION

A natural choice in formulating the objective function for the parameter extraction phase of space mapping is to use the responses for which the specifications are given. In the case of the H-plane filter they are $|S_{11}|$ in dB at selected passband frequencies, and thus the individual errors could be formed by subtracting $|S_{11}|$ in dB from the corresponding specifications (also in dB). A good choice of the objective function for parameter extraction is the ℓ_1 norm of the error vector. We are, however, free to use any error formulation that could allow us to align the models. The results reported

in the preceding section were obtained using $|S_{21}|$. With that formulation the space mapping iterations proceeded flawlessly. No difficulty in the parameter extraction phase could be noticed.

We also took a close look at the ℓ_1 objective function using some other error formulations. Fig. 6 shows two cases of the ℓ_1 norm for parameter extraction during the second iteration of space mapping. They are determined in the vicinity of the starting point w.r.t. two selected parameters: the iris openings d_1 and d_2 . Fig. 6(a) corresponds to the error definition in terms of $|S_{11}|$ (dB). It exhibits many local minima and provides us with an excellent opportunity to investigate the uniqueness of the parameter extraction phase in space mapping, as well as to improve its robustness. When the errors are defined in terms of $|S_{21}|$ (as was used to obtain the space mapping results reported in Section III), the corresponding function surface becomes significantly smoother, as shown in Fig. 6(b).

V. STATISTICAL PARAMETER EXTRACTION

We propose an automated statistical parameter extraction procedure to overcome potential pitfalls arising out of inaccurate or nonunique solutions. First, we perform standard ℓ_1 parameter extraction [15] of the \mathbf{X}_{os} model starting from \mathbf{x}_{os}^* . If the resulting response matches well the \mathbf{X}_{em} model response (the ℓ_1 error is small enough) we continue with the space mapping iterations. Otherwise we turn to statistical exploration of the \mathbf{X}_{os} model.

The key to statistical parameter extraction is to establish the exploration region. Unlike general purpose random/global optimization approaches we want to carry out local statistical exploration as deemed suitable for space mapping. To this end we take advantage of the fact that during the space mapping iterations the desired parameter extraction solutions should rapidly approach \mathbf{x}_{os}^* in the \mathbf{X}_{os} space (see [5,16]).

Consider the k th space mapping iteration. When the current mapping ($\mathbf{x}_{os} = P^{(k-1)}(\mathbf{x}_{em})$) is applied to the current point in the \mathbf{X}_{em} model space we arrive at \mathbf{x}_{os}^* , since that point has been determined by the inverse mapping ($\mathbf{x}_{em}^k = P^{(k-1)^{-1}}(\mathbf{x}_{os}^*)$, see [5]). The fact that the new point (to be extracted) will be different from \mathbf{x}_{os}^* is not only a basis for modifying the mapping, but also it quantitatively establishes the degree of inconsistency w.r.t. the existing mapping. This allows us to define an appropriate exploration region. If, for the k th step, we define the multidimensional interval δ as

$$\delta = \mathbf{x}_{os}^{k-1} - \mathbf{x}_{os}^* \quad (1)$$

the statistical exploration may be limited to the region defined by

$$x_{osi} \in [x_{osi}^* - 2 | \delta_i |, x_{osi}^* + 2 | \delta_i |] \quad (2)$$

Another choice for the exploration region could be an elliptical multidimensional domain with semiaxes $2 | \delta_i |$ defined by

$$\sum_i (x_{osi} - x_{osi}^*)^2 / | \delta_i |^2 \leq 4 \quad (3)$$

A set of N_s starting points is then statistically generated within the region (2) or (3) and N_s parameter extraction optimizations are carried out. These parameter extractions are further aided by a penalty function [16] of the form

$$\lambda \| \mathbf{x}_{os}^k - \mathbf{x}_{os}^* \| \quad (4)$$

augmenting the ℓ_1 objective function. In the case of multiple minima this penalty term forces the optimizer to select local minima closer to \mathbf{x}_{os}^* . The resulting solutions (expected to be multiple) are then categorized into clusters and ranked according to the achieved values of the error function. Finally, the penalty term is removed and the process repeated in order to focus the clustered solution(s). Absence of the penalty term brings the solution point to the "true" local minimum, thus removes "fuzziness" which may occur when the penalty term is used. The aforementioned steps are briefly summarized by the following algorithm and illustrated in the flow chart shown in Fig. 7.

Algorithm

- Step 1* Initialize the exploration region. (2) or (3) can be used in the second and all subsequent space mapping iterations.
- Step 2* Generate N_s random starting points.
- Step 3* Perform N_s parameter extractions from the N_s starting points including the penalty function (4).
- Step 4* Categorize the solutions. Select one or more best clusters of the solutions.
- Step 5* Focus the clusters by reoptimizing without the penalty term.

This approach has been automated by adding one more level in the Datapipe architecture described in Section II. Furthermore, it can be parallelized since the N_s parameter extractions considered are carried out independently.

VI. PARAMETER EXTRACTION OF THE H-PLANE FILTER

We use the H-plane filter example to investigate the statistical parameter extraction outlined in the preceding section. To verify the robustness of the approach we have used the ℓ_1 objective function with various definitions of individual errors. The case when the individual errors are defined in terms of $|S_{11}|$ in dB was already illustrated by Fig. 6(a) for the second iteration of space mapping.

Fig. 8 presents the variation of the MM/network theory model response in the vicinity of the starting point. Responses are computed along the direction of the first aggressive space mapping step, defined by points \mathbf{x}_{os}^* and \mathbf{x}_{os}^1 . Although the responses shown in Fig. 8 are all smooth when only one parameter is varied, the ℓ_1 objective function defined in terms of $|S_{11}|$ (dB) has multiple minima, hence the optimizer may terminate at an undesirable solution.

A set of 100 starting points is statistically generated from a uniform distribution within the range (2). The corresponding 100 ℓ_1 parameter extraction optimizations with the penalty term (4) are then performed from these points. The distances between the point \mathbf{x}_{os}^* and the random starting points are depicted in Fig. 9(a). Correspondingly, the distances between \mathbf{x}_{os}^* and the solutions of parameter extraction optimizations based on the errors defined in terms of $|S_{11}|$ in dB are shown in Fig. 9(b). The solutions are scattered, confirming our observation that the ℓ_1 objective function has many local minima, as illustrated in Fig. 6(a). Among the 100 solutions a cluster of 15 points is detected in Fig. 9(b). Removing the penalty term and restarting the parameter extraction process from all these points further sharpens the solution. All the points within the cluster converge to the same solution, as depicted in Fig. 9(c). Figs. 10

and 11 show the responses of the the \mathbf{X}_{os} model at those 100 points before and after parameter extraction, respectively. Fig. 12 displays the responses corresponding to the cluster of 15 points which converged to the same solution, validating successful parameter extraction.

Fig. 13 illustrates the impact of the penalty term. When the penalty term is not used, only 10 parameter extractions lead to the desired solution, as shown in Fig. 13(a). Here $|S_{11}|$ in dB is used to define the errors. Figs. 13(b) and 13(c) present the results when the errors are defined in terms of $|S_{21}|$. Without the penalty term the procedure leads to 52 successful parameter extractions (Fig. 13(a)); adding the penalty term (4) yields 100% success (Fig. 13(c)). The corresponding responses at the solutions are shown in Fig. 14. Note that for this case of using $|S_{21}|$ in error definition, starting from the default point, \mathbf{x}_{os}^* , yields the correct result. This explain flawless space mapping iterations reported in Section III.

Certainly that definition in terms of scattering coefficient in dB had amplified the error in computed parameter S_{11} . The relative error for such case is higher since S_{11} is small in the pass-band region, and de-facto this approach has implication that optimizer is giving more significance to points with higher error than to more accurate points. We have shown that even for such numerically sensitive case our new procedure guarantee successful parameter extraction.

VII. MULTI-POINT PARAMETER EXTRACTION

We use the two-section waveguide transformer example [17] to further investigate the impact of parameter extraction uniqueness on the convergence of the space mapping iterations. We observe symmetrical ℓ_1 contours with respect to the two section lengths L_1 and L_2 , as illustrated in Fig. 15, with two local minima. Consequently the result of parameter extraction is not unique. The impact can be seen in the trace depicted in Fig. 16, where the space mapping steps oscillate around the solution due to the "fuzzy" results of parameter extraction.

We introduce a multi-point parameter extraction approach to sharpen the parameter extraction result. Instead of minimizing

$$|| \mathbf{R}_{os}(\mathbf{x}_{os}^i) - \mathbf{R}_{em}(\mathbf{x}_{em}^i) || \quad (5)$$

at a single point, we find \mathbf{x}_{os}^i by minimizing

$$|| \mathbf{R}_{os}(\mathbf{x}_{os}^i + \Delta\mathbf{x}) - \mathbf{R}_{em}(\mathbf{x}_{em}^i + \Delta\mathbf{x}) || \quad (6)$$

where $\Delta\mathbf{x}$ represents a small perturbation to \mathbf{x}_{os}^i and \mathbf{x}_{em}^i . By simultaneously minimizing (6) with a selected set of $\Delta\mathbf{x}$,

we hope to improve the uniqueness of the parameter extraction process. Conceptually, we are attempting to match not only the response, but also a first-order change in the response with respect to small perturbations in the parameter values. We have exploited a similar concept in multi-circuit modeling [18]. Fig. 17 depicts the ℓ_1 contours for multi-point parameter extraction of the two-section transformer, which indicates a unique solution. We used three points (i.e., original \mathbf{x}_{em}^i and two perturbations in L_1 and L_2 directions) for parameter extraction. The corresponding space mapping trace is shown in Fig. 18, where the convergence of the space mapping iterations is dramatically improved. The price we may have to pay for such an improvement might be the increased number of \mathbf{X}_{em} simulations required: although more \mathbf{X}_{em} model simulations are needed in parameter extraction, the overall number of iterations may be reduced.

VIII. TOLERANCE SIMULATION USING SPACE MAPPING

Space mapping provides not only the optimized parameter values, but also an efficient means of statistical tolerance analysis. We can map parameter tolerances in the \mathbf{X}_{em} space to the corresponding incremental changes in the \mathbf{X}_{os} space. Consequently, we will be able to rapidly estimate the effects of manufacturing tolerances, benefitting at the same time from the accuracy of the FEM model and the speed of the hybrid MM/network theory simulations.

As an illustration, we consider Monte Carlo analysis of the H-plane filter. We assign normally distributed tolerances to all parameter values, with a standard deviation of 0.0333% (of the order of 1 μm). The Monte Carlo simulation results are shown in Fig. 19. Assuming a specification of $|S_{11}|$ (dB) < -15 in the passband, the estimated yield is 88.5% out of 200 outcomes. Then, we increased the standard deviations of the parameter tolerances to 0.1%. This time the yield dropped to 19% out of 200 outcomes.

By using the space mapping model, the CPU time required for the Monte Carlo analysis is comparable to just a single full FEM simulation.

IX. SPACE MAPPING OPTIMIZATION USING COARSE AND FINE MM MODELS

The RWGMM library allows a designer to take into account a large number of higher-order modes to model waveguide transition components. Increasing the number of modes improves accuracy at the expense of higher computational cost. Space mapping may enhance the efficiency of the MM-based optimization by aligning the response of the fine model (including many modes) with the response of a coarse model (using one or a few modes).

We apply this strategy to the optimization of three-section and seven-section transformers described in [17]. For the coarse model, we used just one mode. For the fine model, we included all the modes below the cut-off frequency $f = 50$ GHz. The actual number of modes included in the fine model is automatically determined by the RWGMM program. As the lengths and heights of the waveguide sections are optimized, the number of modes included in the fine model varies from 49 to 198 for the three-section and at least 180 for the seven-section transformer. The optimized solutions shown in Figs. 20 and 21 require two and 14 space mapping iterations, respectively.

X. CONCLUSIONS

We have presented new applications of aggressive space mapping to filter optimization using network theory, mode-matching and finite element simulation techniques. A statistical approach to parameter extraction incorporating the ℓ_1 error and penalty function concepts has effectively addressed the requirement of a unique and consistent solution. We have introduced the multi-point approach to enhancing the prospect of a unique parameter extraction solution in the space mapping process. Among important extensions of this work we envisage a highly efficient means for Monte Carlo analysis of microwave circuits carried out with the accuracy of FEM simulation. We have also demonstrated space mapping optimization based on coarse and fine MM models with different numbers of modes.

ACKNOWLEDGEMENTS

The authors would like to thank Ansoft Corp. of Pittsburgh, PA, and Prof. Fritz Arndt of the University of Bremen, Germany, for making their respective software available for this work.

REFERENCES

- [1] J.W. Bandler, R.M. Biernacki, S.H. Chen and D. Omeragić, "Electromagnetic optimization of 3D structures," to appear in *IEEE Trans. Microwave Theory Tech.*, vol. 45, May 1997.
- [2] F. Arndt, S.H. Chen, W.J.R. Hoefer, N. Jain, R.H. Jansen, A.M. Pavio, R.A. Pucel, R. Sorrentino and D.G. Swanson, Jr., *Automated Circuit Design using Electromagnetic Simulators*. Workshop WMFE (J.W. Bandler and R. Sorrentino, Organizers and Chairmen), IEEE MTT-S Int. Microwave Symp., Orlando, FL, May 1995.
- [3] J.W. Bandler, R.M. Biernacki and S.H. Chen, "Fully automated space mapping optimization of 3D structures," *IEEE MTT-S Int. Microwave Symp. Dig.*, San Francisco, CA, pp. 753-756, June 1996.
- [4] J.W. Bandler, R.M. Biernacki, S.H. Chen, P.A. Grobelny and R.H. Hemmers, "Space mapping technique for

- electromagnetic optimization," *IEEE Trans. Microwave Theory Tech.*, vol. 42, pp. 2536-2544, December 1994.
- [5] J.W. Bandler, R.M. Biernacki, S.H. Chen, R.H. Hemmers and K. Madsen, "Electromagnetic optimization exploiting aggressive space mapping," *IEEE Trans. Microwave Theory Tech.*, vol. 43, pp. 2874-2882, December 1995.
- [6] T. Sieverding, U. Papziner, T. Wolf and F. Arndt, "New mode-matching building blocks for common circuit CAD programs," *Microwave Journal*, vol. 36, pp. 66-79, July 1993.
- [7] F. Arndt, T. Sieverding, T. Wolf and U. Papziner, "Optimization-oriented design of rectangular and circular waveguide components using efficient mode-matching simulators in commercial circuit CAD tools," *Int. J. Microwave and Millimeter-Wave Computer-Aided Engineering*, vol. 7, pp. 37-51, January 1997.
- [8] F. Alessandri, M. Dionigi and R. Sorrentino, "A fullwave CAD tool for waveguide components using a high speed direct optimizer," *IEEE Trans. Microwave Theory Tech.*, vol. 43, pp. 2046-2052, December 1995.
- [9] *OSA90/hope*TM and *Empipe3D*TM, Optimization Systems Associates Inc., P.O. Box 8083, Dundas, Ontario, Canada L9H 5E7.
- [10] *Maxwell Eminence*, Ansoft Corporation, Four Station Square, Suite 660, Pittsburgh, PA 15219, USA.
- [11] P.P. Silvester and G. Pelosi, *Finite elements for wave electromagnetics, methods and techniques*. New York: IEEE Press, 1994.
- [12] J.-F. Lee, D.-K. Sun and Z.J. Cendes, "Full-wave analysis of dielectric waveguides using tangential vector finite elements," *IEEE Trans. Microwave Theory Tech.*, vol. 39, pp. 1262-1271, August 1991.
- [13] J.W. Bandler, R.M. Biernacki, S.H. Chen and P.A. Grobelny, "Optimization technology for nonlinear microwave circuits integrating electromagnetic simulations," *Int. J. Microwave and Millimeter-Wave Computer-Aided Engineering*, vol. 7, pp. 6-28 January 1997.
- [14] F. Arndt, Microwave Department, University of Bremen, P.O. Box 330 440, Kufsteiner Str., NW1, D-28334 Bremen, Germany, 1996, *private communications*.
- [15] J.W. Bandler, S.H. Chen and S. Daijavad, "Microwave device modeling using efficient ℓ_1 optimization: a novel approach," *IEEE Trans. Microwave Theory Tech.*, vol. MTT-34, pp. 1282-1293, December 1986.
- [16] J.W. Bandler, R.M. Biernacki, S.H. Chen and Y.F. Huang, "Design optimization of interdigital filters using aggressive space mapping and decomposition," to appear in *IEEE Trans. Microwave Theory Tech.*, vol. 45, May 1997.
- [17] J.W. Bandler, "Computer optimization of inhomogeneous waveguide transformers," *IEEE Trans. Microwave Theory Tech.*, vol. MTT-17, pp. 563-571, August 1969.
- [18] J.W. Bandler and S.H. Chen, "Circuit optimization: the state of the art," *IEEE Trans. Microwave Theory Tech.*, vol. 36, pp. 424-443, February 1988.

TABLE I
SPACE MAPPING OPTIMIZATION OF THE H-PLANE FILTER

Point	d_1	d_2	l_1	l_2
\mathbf{x}_{em}^1	6.04541	3.21811	13.0688	13.8841
\mathbf{x}_{em}^2	6.19267	3.32269	12.9876	13.8752
\mathbf{x}_{em}^3	6.17017	3.29692	13.0536	13.8812
\mathbf{x}_{em}^4	6.17557	3.29058	13.0282	13.8841

Values of all optimization variables are in mm.

TABLE II
PARAMETER EXTRACTION RESULTS FOR SPACE MAPPING OPTIMIZATION

Point	d_1	d_2	l_1	l_2	$\ \mathbf{x}_{os}^* - \mathbf{x}_{os}^i \ $
\mathbf{x}_{os}^1	5.89815	3.11353	13.1500	13.8930	0.19823
\mathbf{x}_{os}^2	6.07714	3.25445	12.9757	13.8757	0.10519
\mathbf{x}_{os}^3	6.03531	3.22421	13.1119	13.8806	0.04482
\mathbf{x}_{os}^4	6.04634	3.22042	13.0618	13.8831	0.00750

Values of all optimization variables are in mm.

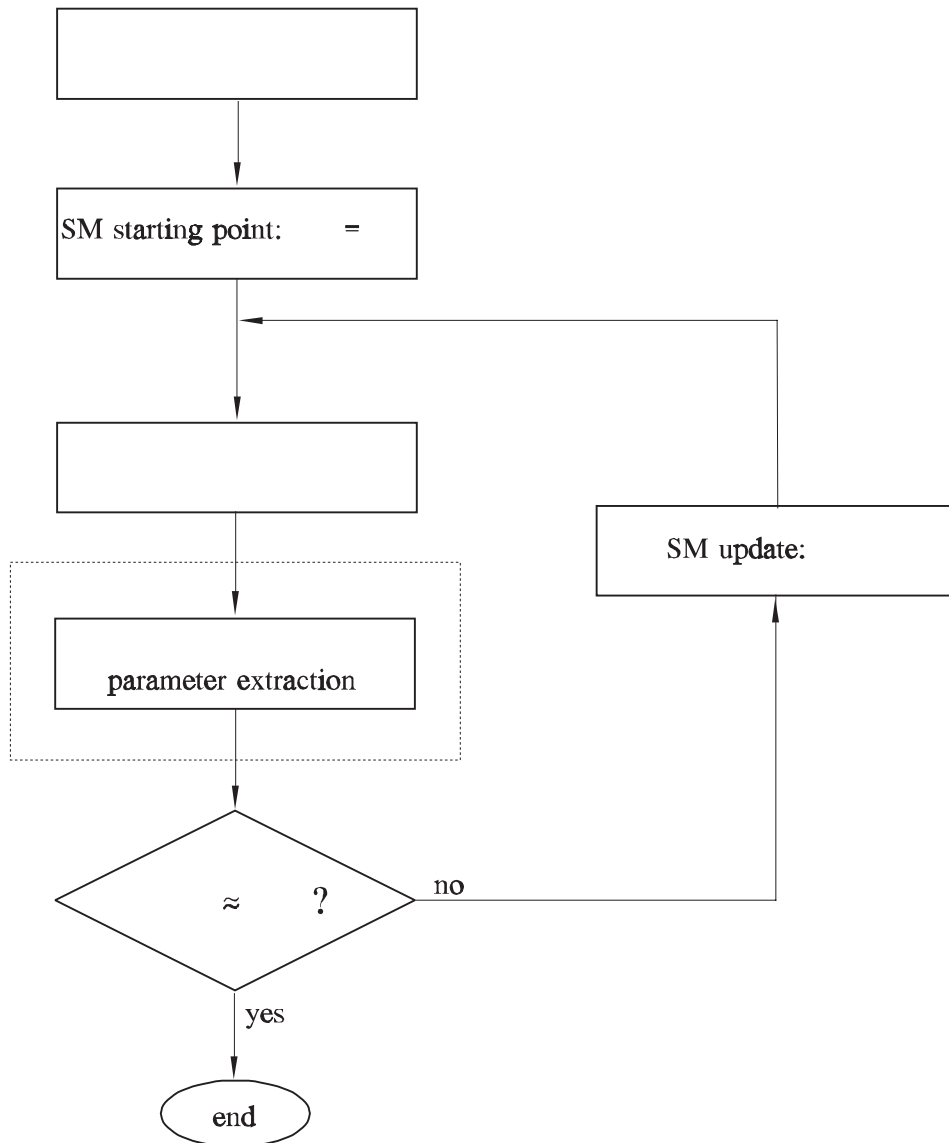
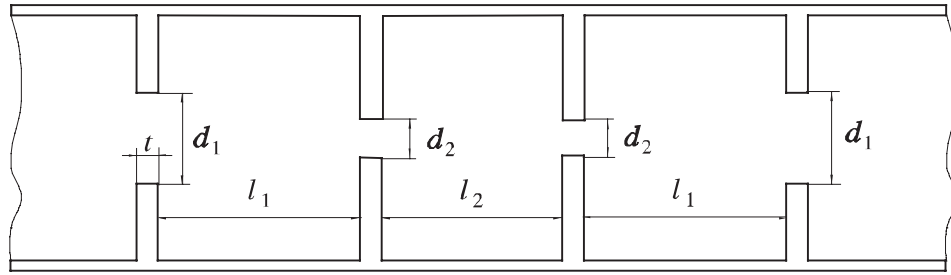
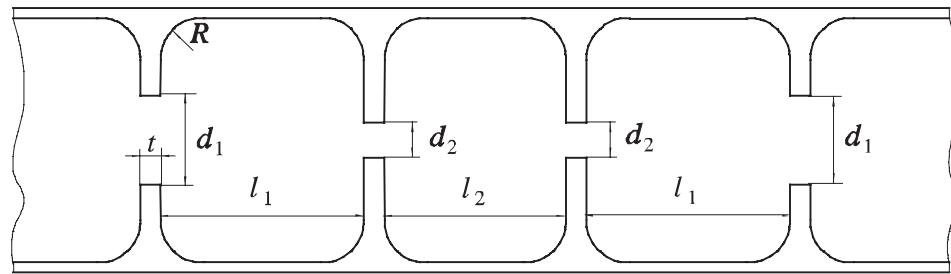


Fig. 1. Flow diagram of the space mapping optimization (SM) procedure concurrently exploiting the hybrid MM/network theory and FEM techniques and statistical parameter extraction.



(a)



(b)

Fig. 2. Structures for space mapping optimization: (a) optimization space model, for hybrid MM/network theory; (b) fine model, for analysis by FEM. The waveguide cross-section is 15.8×7.9 mm, the thickness of the irises is $t = 0.4$ mm. Optimization variables are iris openings d_1 , d_2 and resonator lengths l_1 , l_2 .

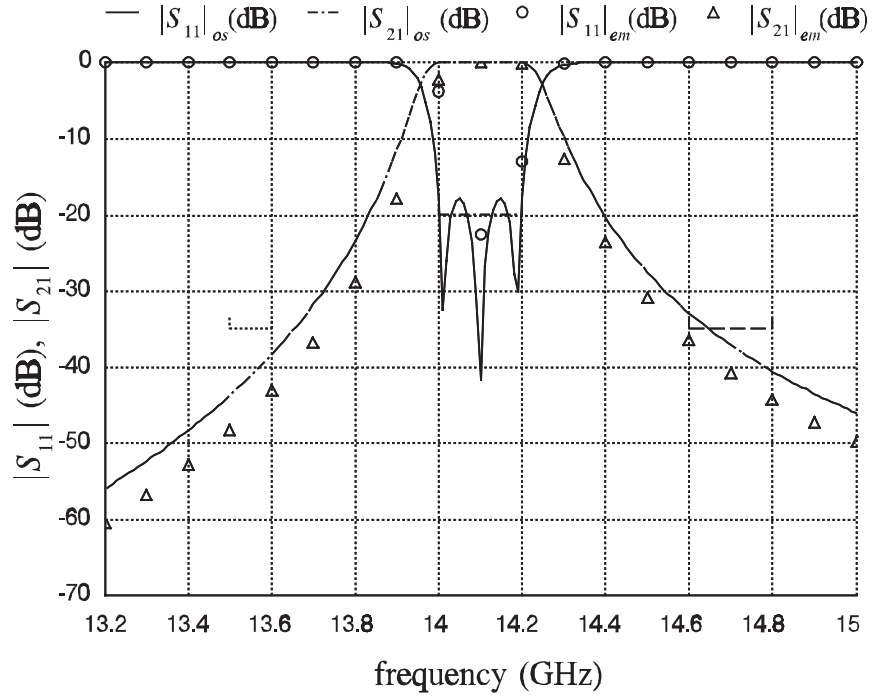


Fig. 3. Responses from both simulations of the H-plane filter based on the hybrid MM/network theory optimization solution before space mapping optimization.

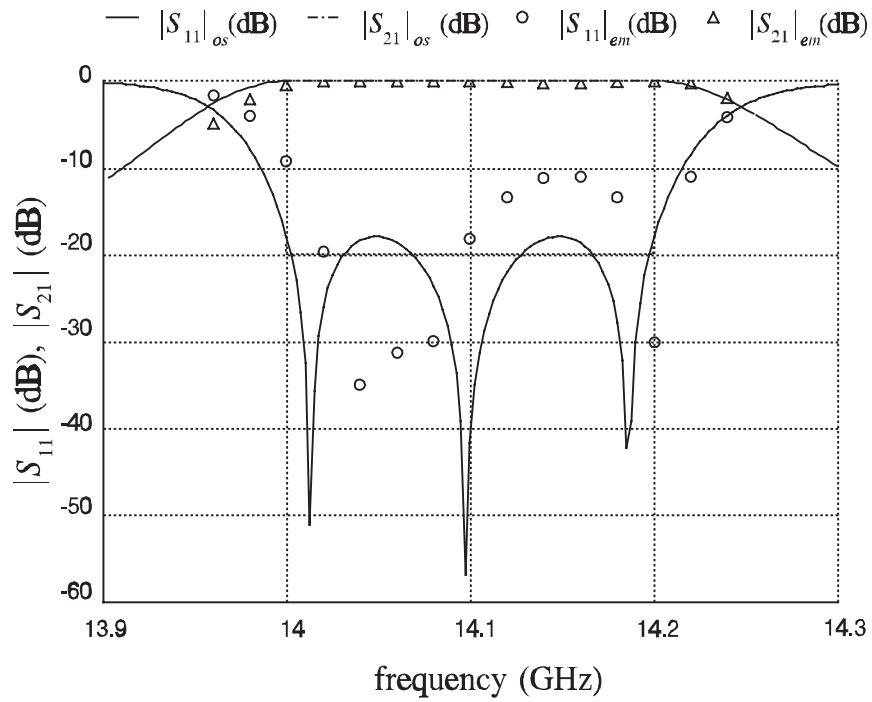


Fig. 4. Responses from both simulations of the H-plane filter before space mapping optimization, focusing on the passband.

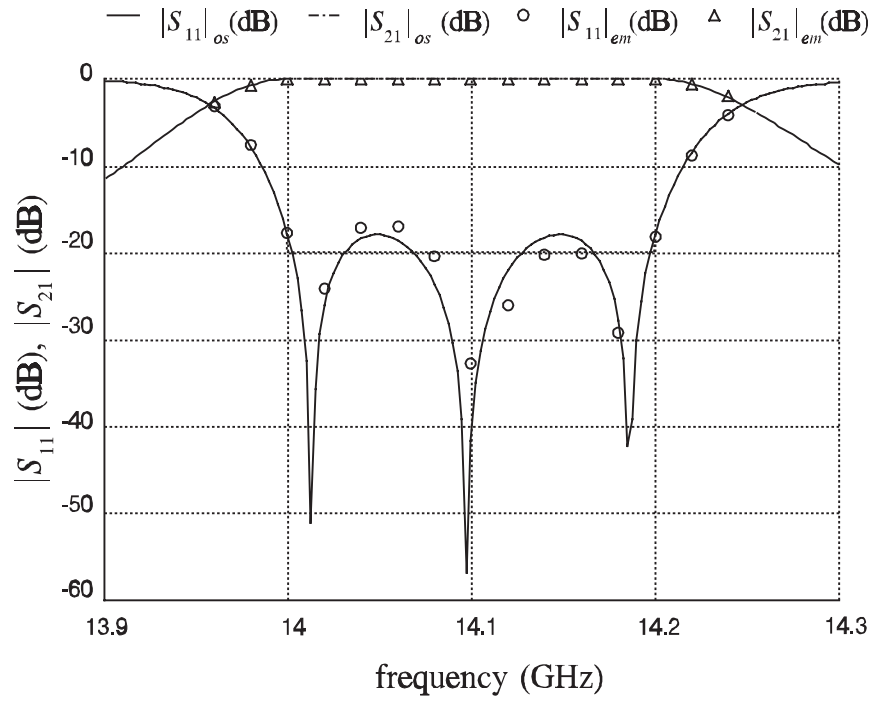
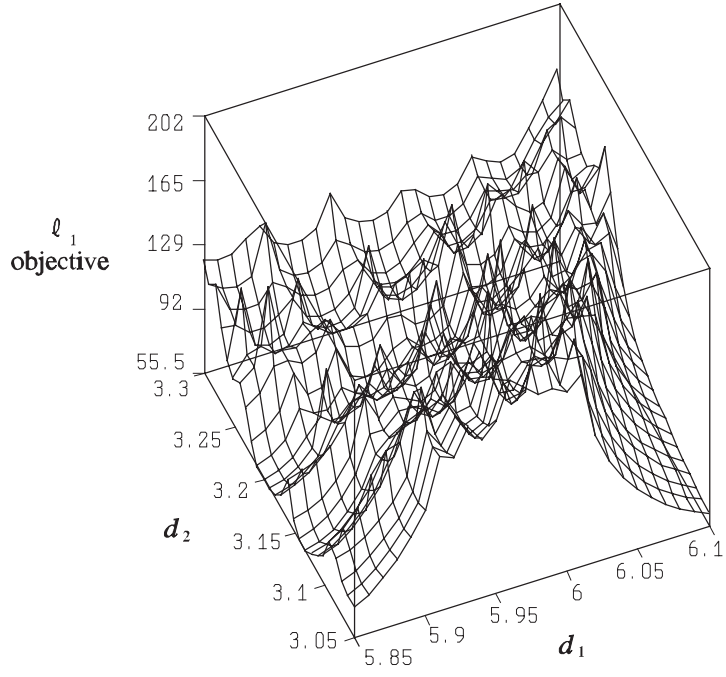
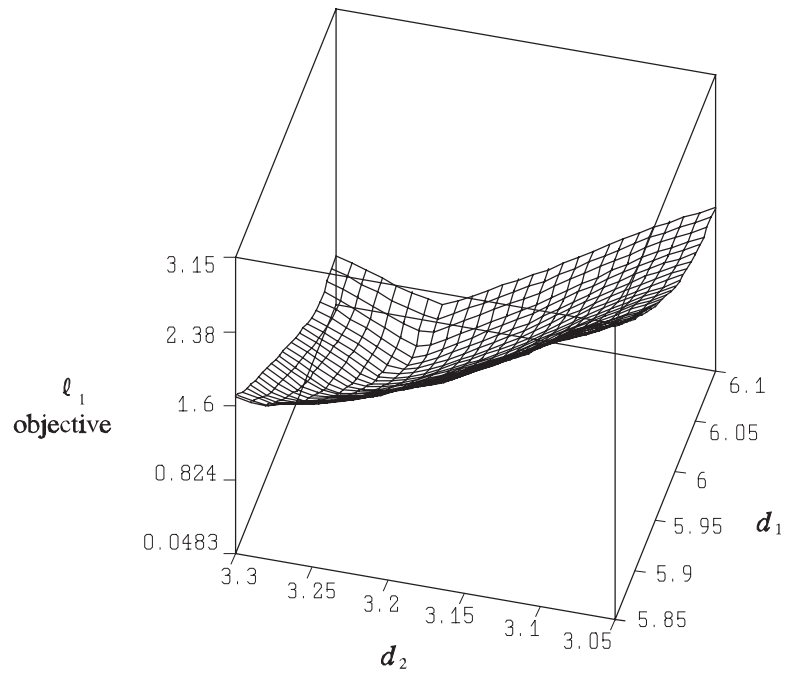


Fig. 5. Space mapping optimized FEM response of the H-plane filter compared with the optimal X_{os} response target. Optimal results have been obtained after only 4 simulations by Maxwell Eminence.



(a)



(b)

Fig. 6. Variation of l_1 error w.r.t. iris openings d_1 and d_2 . Other parameters were held fixed at values corresponding to \mathbf{x}_{os}^* . Error function defined in terms of: (a) $|S_{11}|$ (dB); (b) $|S_{21}|$.

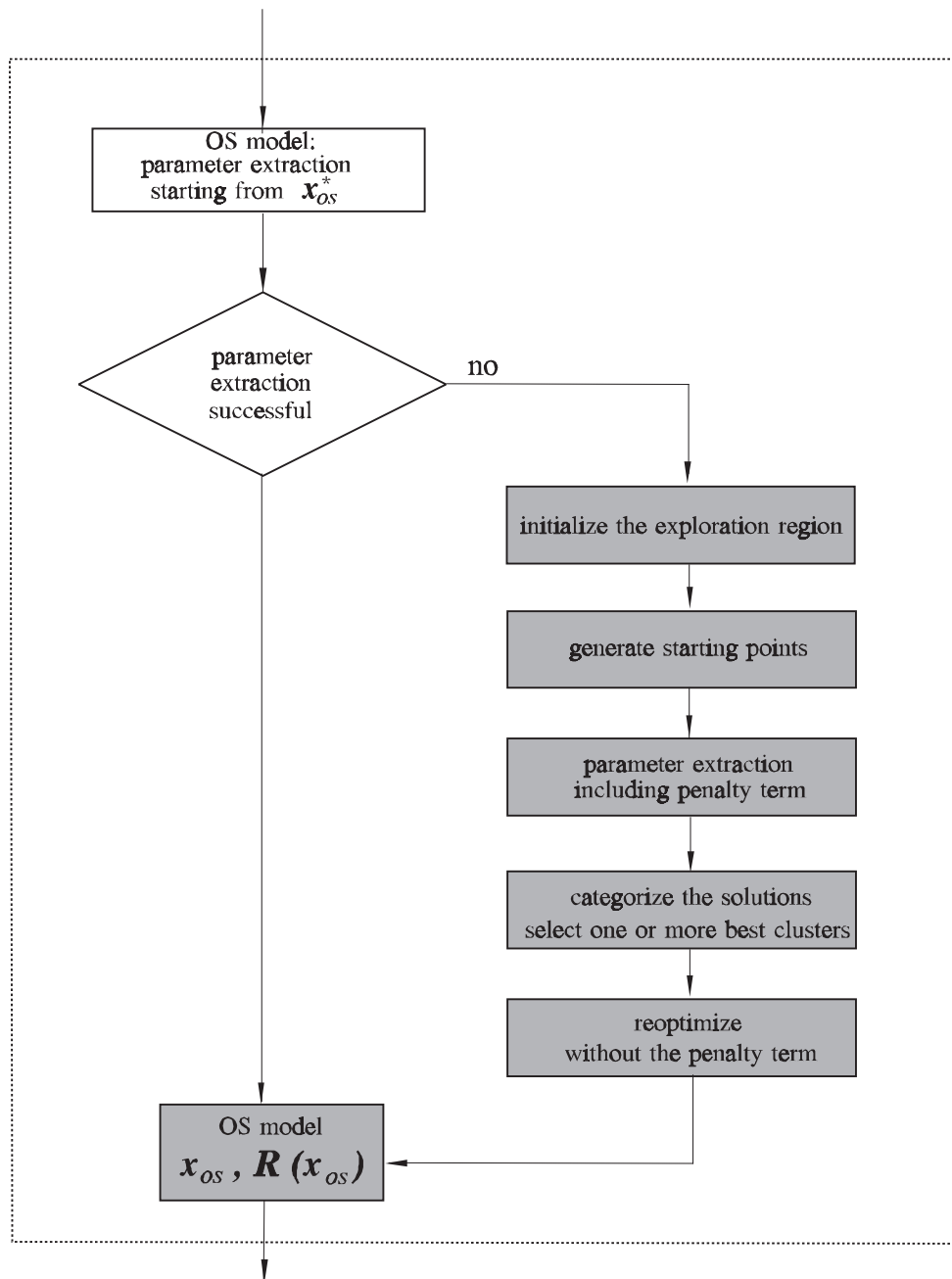


Fig. 7. Flow diagram of the statistical parameter extraction procedure.

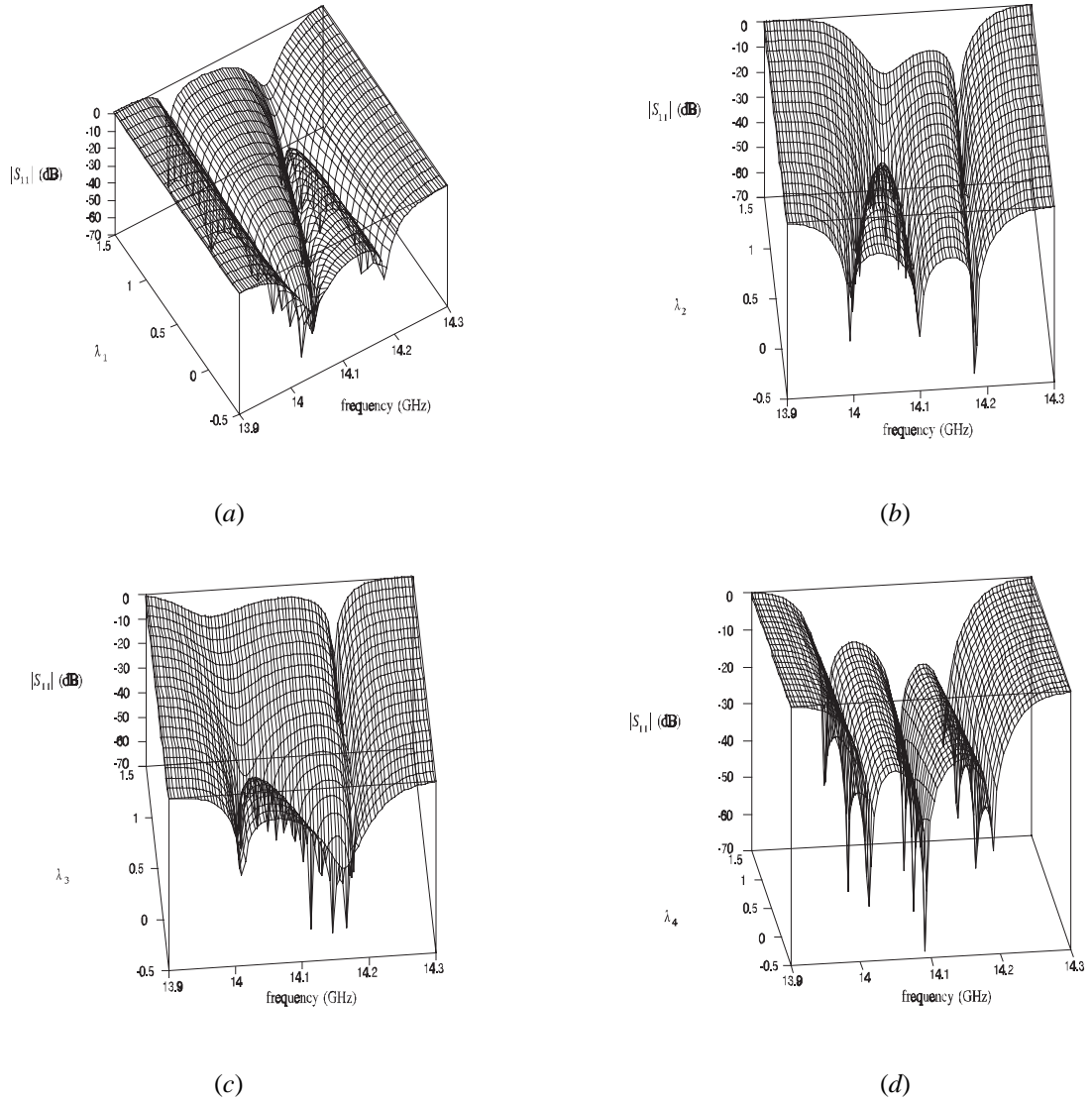
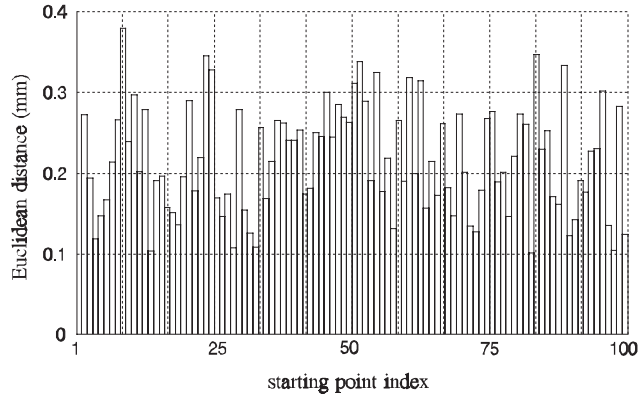
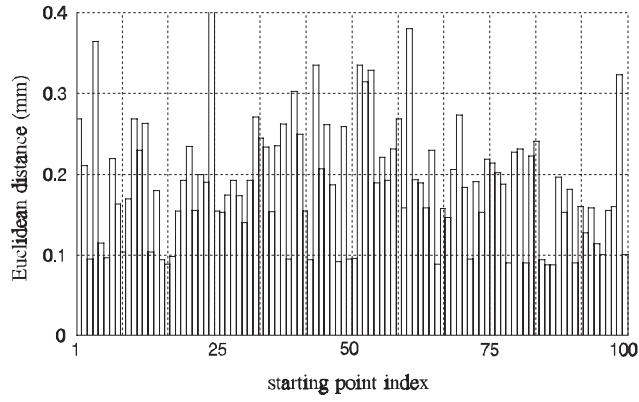


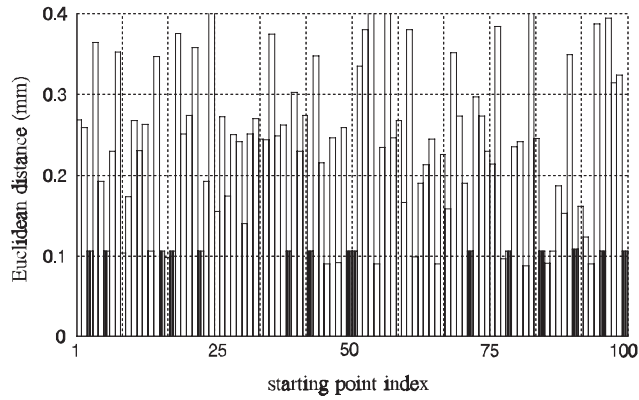
Fig. 8. Variation of responses w.r.t. each parameter, with total changes defined by the first space mapping step. $\lambda_i = 0$ at \mathbf{x}_{os}^* and $\lambda_i = 1$ at \mathbf{x}_{os}^1 . Variation of: (a) opening of the first iris, d_1 ; (b) opening of the second iris, d_2 ; (c) length of the first resonator; (d) length of the second resonator.



(a)



(b)



(c)

Fig. 9. Statistical parameter extraction: (a) Euclidean distances of the starting points generated randomly; (b) Euclidean distances of converged point after the first step; (c) Euclidean distances of converged point after the second stage of statistical parameter extraction. All distances are measured from the standard starting point \mathbf{x}_{os}^* . Error function defined in terms of $|S_{11}|$ (dB).

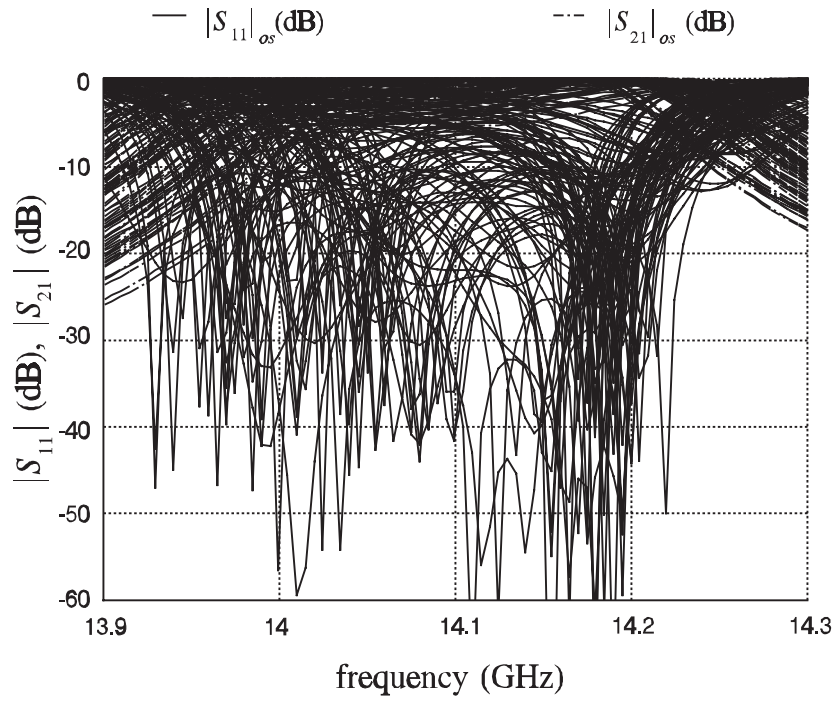


Fig. 10. Statistical parameter extraction: responses at 100 starting points generated randomly by perturbing parameters of the standard starting point.

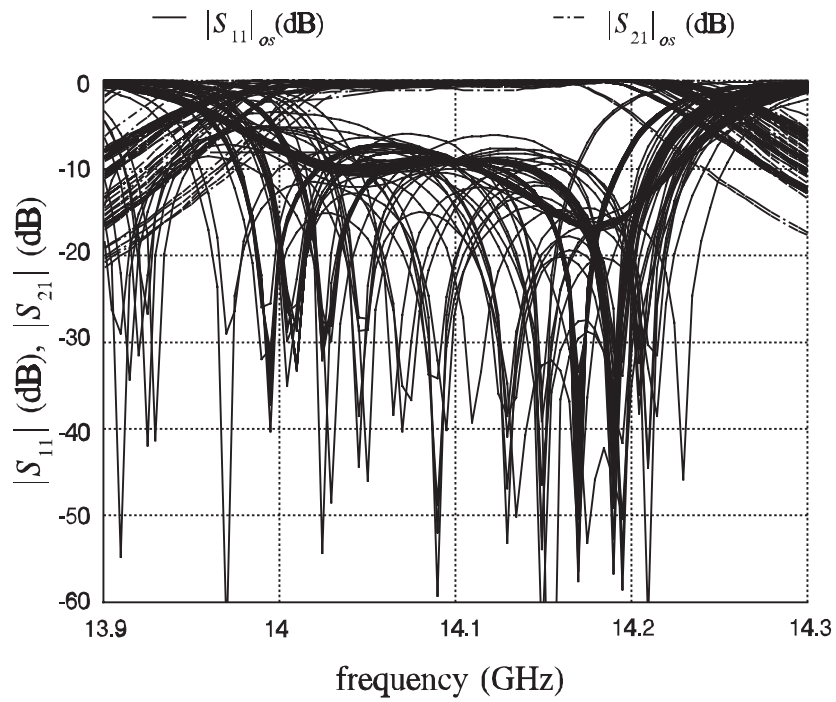


Fig. 11. Statistical parameter extraction: responses at 100 parameter extraction solution points.

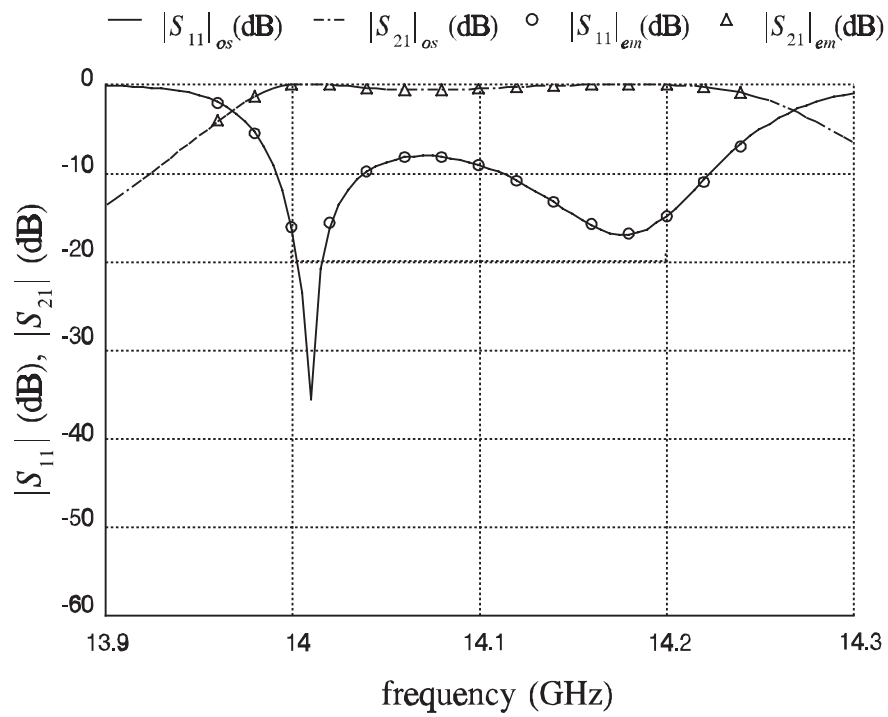
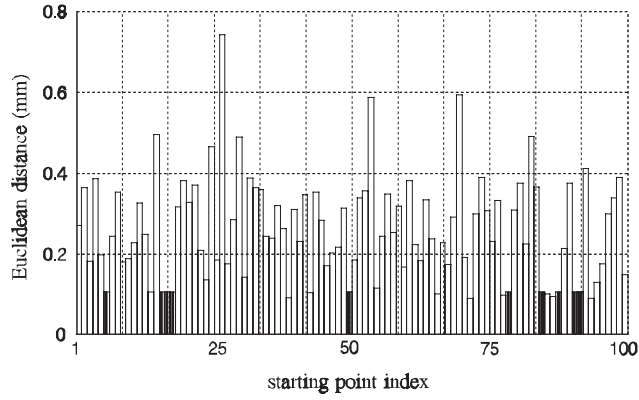
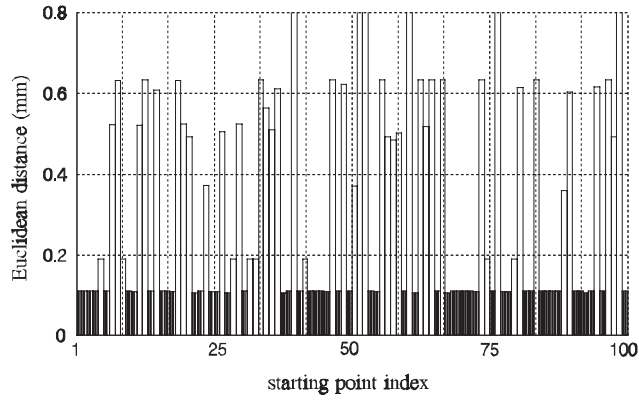


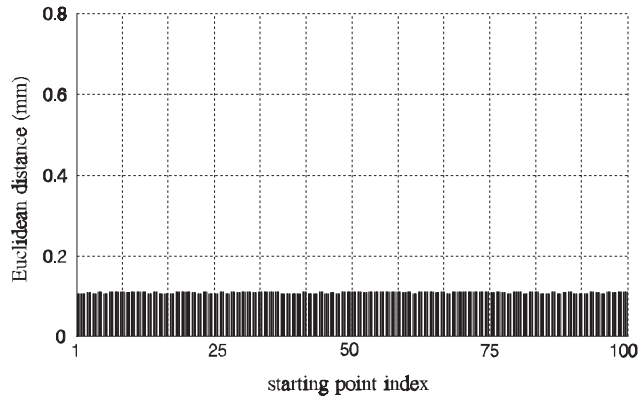
Fig. 12. MM responses corresponding to a cluster of 15 converged points obtained after statistical parameter extraction. The match to the FEM response is very good. The 15 responses are indistinguishable from each other.



(a)



(b)



(c)

Fig. 13. Statistical parameter extraction. Euclidean distances of converged point after the second stage of statistical parameter extraction: (a) Error function defined in terms of $|S_{11}|$ (dB), no penalty term (4) used; (b) Error function defined in terms of $|S_{21}|$, no penalty term (4) used; (c) Error function defined in terms of $|S_{21}|$, penalty term (4) used. All distances are measured from the standard starting point \mathbf{x}_{os}^* .

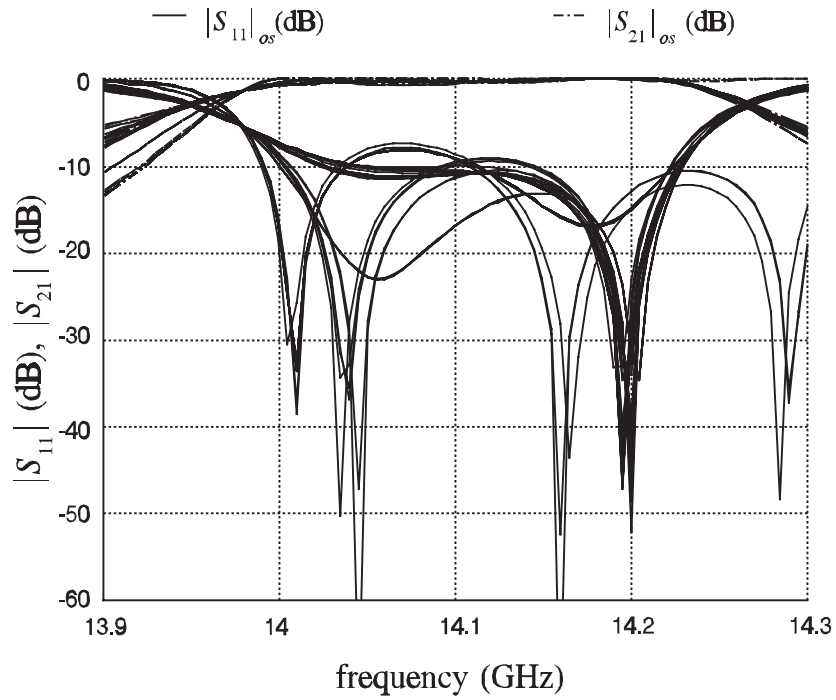


Fig. 14. Statistical parameter extraction: responses at 100 parameter extraction solution points. No penalty term (4) used. Error function defined in terms of $|S_{21}|$.

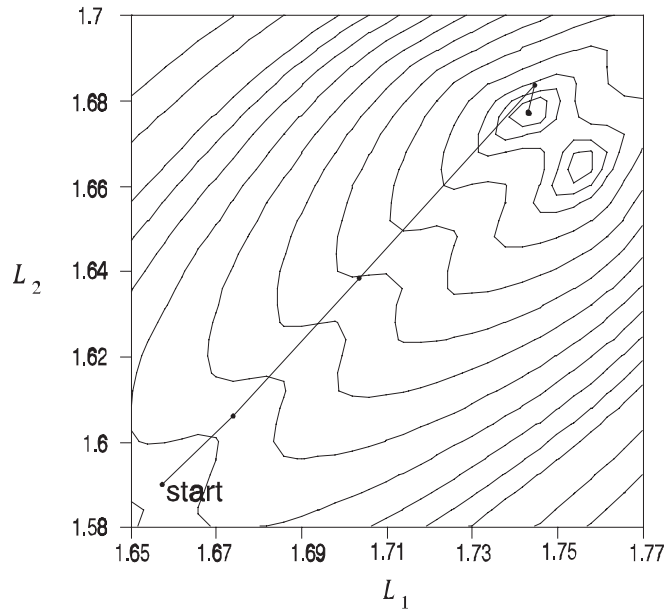


Fig. 15. The ℓ_1 contours of the parameter extraction problem for the two-section waveguide transformer. The symmetry between the variables L_1 and L_2 produces two local minima. Consequently the result of parameter extraction is not unique.

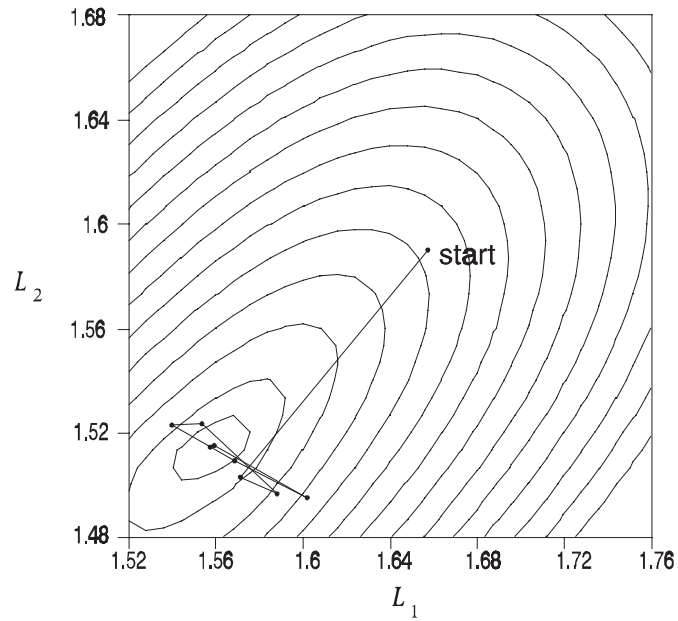


Fig. 16. Trace of the space mapping steps of the two-section waveguide transformer projected onto the minimax contours in the L_1 - L_2 plane. The non-unique parameter extraction results lead to the space mapping steps oscillating around the solution.

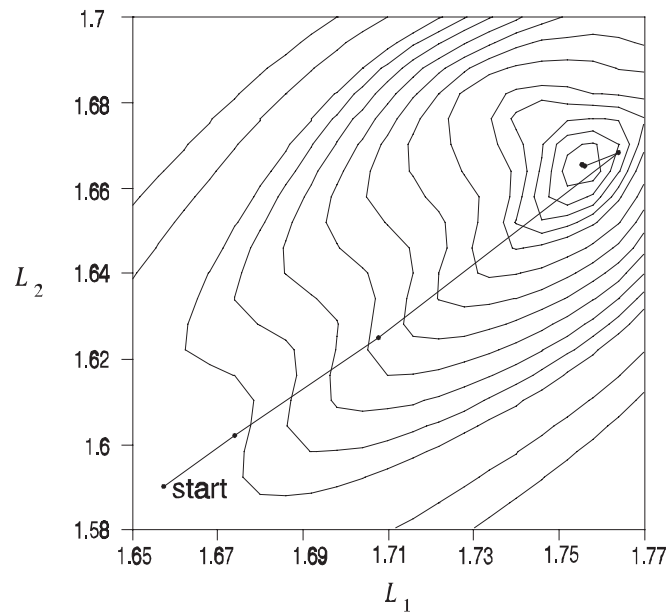


Fig. 17. The ℓ_1 contours of multi-point parameter extraction of the two-section waveguide transformer. The parameter extraction has a unique solution.

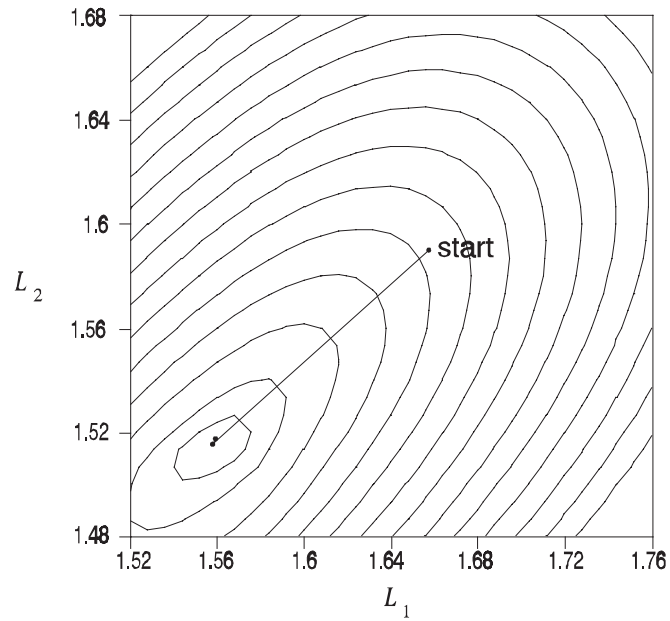


Fig. 18. Trace of the space mapping optimization with multi-point parameter extraction of the two-section transformer projected onto the minimax contours in the L_1 - L_2 plane. The convergence is dramatically improved when compared with Fig. 16.

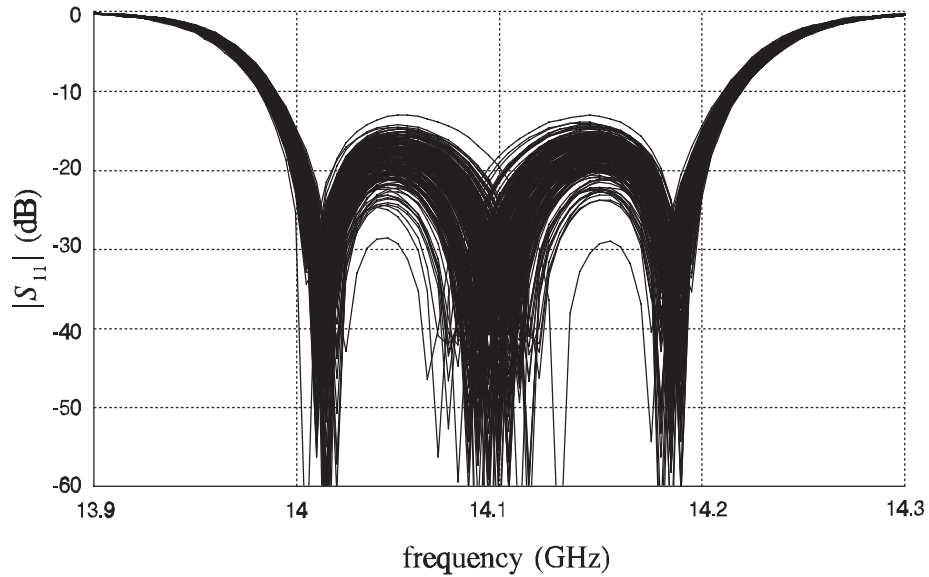


Fig. 19. Monte Carlo analysis of the H-plane filter. The parameter tolerances were statistically generated with a standard deviation of 0.0333%. The estimated yield is 88.5% out of 200 outcomes.

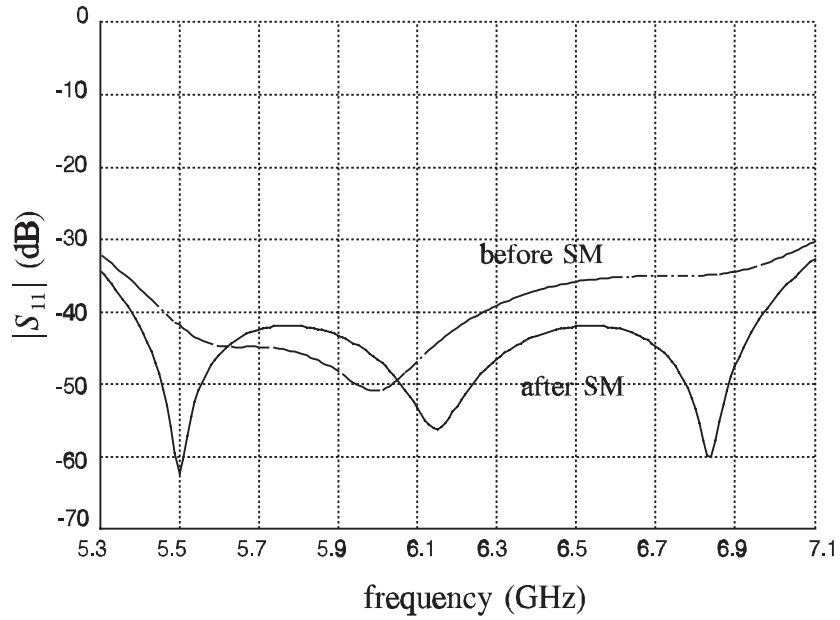


Fig. 20. $|S_{11}|$ (dB) response of a three-section waveguide transformer simulated by RWGMM library before and after two space mapping (SM) optimization steps. The SM solution is indistinguishable from the optimal coarse model response.

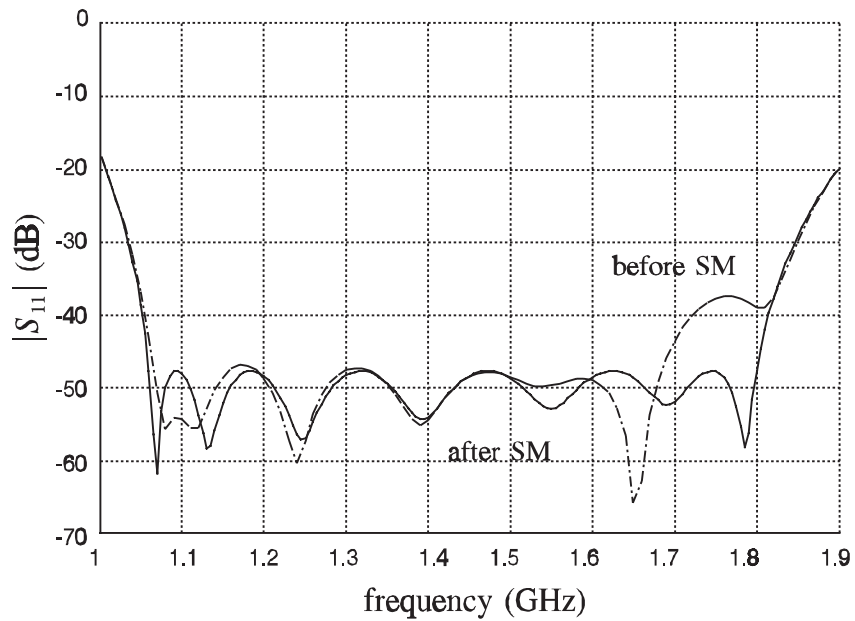


Fig. 21. $|S_{11}|$ (dB) response of a seven-section waveguide transformer simulated by RWGMM library before and after 14 space mapping (SM) optimization steps. The SM solution is indistinguishable from the optimal coarse model response.

Figure Captions

1. Flow diagram of the space mapping optimization (SM) procedure concurrently exploiting the hybrid MM/network theory and FEM techniques and statistical parameter extraction.
2. Structures for space mapping optimization: (a) optimization space model, for hybrid MM/network theory; (b) fine model, for analysis by FEM. The waveguide cross-section is 15.8×7.9 mm, the thickness of the irises is $t = 0.4$ mm. Optimization variables are iris openings d_1, d_2 and resonator lengths l_1, l_2 .
3. Responses from both simulations of the H-plane filter based on the hybrid MM/network theory optimization solution before space mapping optimization.
4. Responses from both simulations of the H-plane filter before space mapping optimization, focusing on the passband.
5. Space mapping optimized FEM response of the H-plane filter compared with the optimal \mathbf{X}_{os} response target. Optimal results have been obtained after only 4 simulations by Maxwell Eminence.
6. Variation of ℓ_1 error w.r.t. iris openings d_1 and d_2 . Other parameters were held fixed at values corresponding to \mathbf{x}_{os}^* . Error function defined in terms of: (a) $|S_{11}|$ (dB); (b) $|S_{21}|$.
7. Flow diagram of the statistical parameter extraction procedure.
8. Variation of responses w.r.t. each parameter, with total changes defined by the first space mapping step. $\lambda_i = 0$ at \mathbf{x}_{os}^* and $\lambda_i = 1$ at \mathbf{x}_{os}^1 . Variation of: (a) opening of the first iris d_1 ; (b) opening of the second iris, d_2 ; (c) length of the first resonator; (d) length of the second resonator.
9. Statistical parameter extraction: (a) Euclidean distances of the starting points generated randomly; (b) Euclidean distances of converged point after the first step; (c) Euclidean distances of converged point after the second stage of statistical parameter extraction. All distances are measured from the standard starting point \mathbf{x}_{os}^* .
10. Statistical parameter extraction: responses at 100 starting points generated randomly by perturbing parameters of the standard starting point.
11. Statistical parameter extraction: responses at 100 parameter extraction solution points.
12. MM responses corresponding to a cluster of 15 converged points obtained after statistical parameter extraction. The match to the FEM response is very good. The 15 responses are indistinguishable from each other.
13. Statistical parameter extraction. Euclidean distances of converged point after the second stage of statistical parameter extraction: (a) Error function defined in terms of $|S_{11}|$ (dB), no penalty term (4) used; (b) Error function defined in terms of $|S_{21}|$, no penalty term (4) used; (c) Error function defined in terms of $|S_{21}|$, penalty term (4) used. All distances are measured from the standard starting point \mathbf{x}_{os}^* .
14. Statistical parameter extraction: responses at 100 parameter extraction solution points. No penalty term (4) used. Error function defined in terms of $|S_{21}|$.
15. The ℓ_1 contours of the parameter extraction problem for the two-section waveguide transformer. The symmetry between the variables L_1 and L_2 produces two local minima. Consequently the result of parameter extraction is not unique.

16. Trace of the space mapping steps of the two-section waveguide transformer projected onto the minimax contours in the L_1 - L_2 plane. The non-unique parameter extraction results lead to the space mapping steps oscillating around the solution.
17. The ℓ_1 contours of multi-point parameter extraction of the two-section waveguide transformer. The parameter extraction has a unique solution.
18. Trace of the space mapping optimization with multi-point parameter extraction of the two-section transformer projected onto the minimax contours in the L_1 - L_2 plane. The convergence is dramatically improved when compared with Fig. 16.
19. Monte Carlo analysis of the H-plane filter. The parameter tolerances were statistically generated with a standard deviation of 0.0333%. The estimated yield is 88.5% out of 200 outcomes.
20. $|S_{11}|$ (dB) response of a three-section waveguide transformer simulated by RWGMM library before and after two space mapping (SM) optimization steps. The SM solution is indistinguishable from the optimal coarse model response.
21. $|S_{11}|$ (dB) response of a seven-section waveguide transformer simulated by RWGMM library before and after 14 space mapping (SM) optimization steps. The SM solution is indistinguishable from the optimal coarse model response.